ELSEVIER

Journal of Photochemistry and Photobiology A: Chemistry 137 (2000) 115–123

Journal of Photochemistry and Photobiology A:Chemistry

www.elsevier.nl/locate/jphotochem

Photophysics of some styryl thiazolo quinoxaline dyes in organic media

A.S.R. Koti [a], B. Bhattacharjee [a], N.S. Haram [a], Ranjan Das [a], N. Periasamy [a,*], N.D. Sonawane [b], D.W. Rangnekar [b]

[a] *Department of Chemical Sciences, Tata Institute of Fundamental Research, Colaba, Mumbai 400 005, India*
[b] *Dyestuff Division, University Department of Chemical Technology, Matunga, Mumbai 400 019, India*

Received 9 May 2000; received in revised form 17 July 2000; accepted 22 August 2000

Abstract

The photophysics of a new class of styryl dyes, 2-styryl thiazolo quinoxaline (STQ) based structures was investigated in organic solvents and organized molecular assemblies. The absorption, steady state and time-resolved fluorescence characteristics of the STQ dyes in low-viscosity organic solvents are consistent with a single species in the ground and excited state. The one electron electrochemical oxidation and reduction potentials of the dyes are within ±1 V vs. NHE. The spectral shifts of the dyes in organic solvents are linearly correlated with the variation of solvent polarity parameters. The dipole moments in the ground and excited state of the dyes were calculated without assuming a value for the cavity radius. The temperature dependence of the nonradiative rate of STQ dye in DMSO indicated an activation barrier ($\Delta E = 10.7$ kJ/mol) which is comparable to the activation energy ($E_a = 13.7$ kJ/mol) of viscous friction in DMSO. In dichloromethane, the activation barrier is 34.0 kJ/mol which is very high compared to $E_a = 6.64$ kJ/mol. Formation of a dye–solvent complex is suggested in dichloromethane.

The fluorescence decay of STQ dye is multiexponential in a viscous solvent (2-octanol) or when bound to a protein (Lysozyme), micelle or lipid membrane. In 2-octanol, the decay parameters are wavelength dependent and the results are consistent with the mechanism of excited state kinetics of solvent relaxation. In other systems, the multiexponential decay is due to multiple sites of solubilization of the dye in the organized molecular assembly.

Keywords: Styryl dyes; Thiazolo quinoxaline dyes; Fluorescence; Organized molecular assemblies

1. Introduction

Conjugated organic dye molecules are recognized to be important materials having novel electronic and photonic properties suitable for many technological applications [1–3]. Synthesis of new organic molecules and characterization of the photophysical molecular properties in different environments (pure solvents and molecular assemblies) are necessary prerequisites for further research in technological applications. The styryl dye with electron donor–acceptor moieties on either side of the styryl bond is particularly attractive for their spectral sensitivity towards local host environment and optical and electronic properties. A number of styryl dyes (styrene-like dyes with different aromatic groups on either side of the styryl double bond) have been synthesized and investigated [4–10]. A few styryl dyes were found to be useful in biological applications [11]. In this paper, we report the photophysical properties of a new class of fluorescent thiazolo quinoxaline based styryl dyes called STQ dyes in organic solvents and organized molecular assemblies.

2. Experimental

The synthesis, purification and characterization of the styryl thiazolo quinoxaline dyes have been described elsewhere [12]. Fig. 1 shows the structure of the three dyes, STQ-1, STQ-2 and STQ-3 used in this study. Rhodamine 101 (Exciton, USA) was used as the fluorescence quantum yield standard. All the solvents used in this study were either Analar or Spectrograde. Sodium dodecyl sulphate (SDS), lysozyme and egg phosphotidyl choline (eggPC) were purchased from Sigma Chemicals, USA.

The samples in organized molecular assemblies were prepared as follows. SDS micelles were prepared by stirring the surfactant (20 mg/ml) in warm deionized water for 1 h. The sonicated, unilamellar eggPC liposomes (0.14 mg/ml) were prepared in buffer pH 7.4 by the procedure described in Ref. [13]. Lysozyme (1 mg/ml) solution was prepared in buffer

* Corresponding author. Fax: +91-22-215-2110/+91-22-215-2181.
E-mail address: peri@tifr.res.in (N. Periasamy).

1010-6030/00/$ – see front matter
PII: S1010-6030(00)00360-9

STRUCTURE OF THE DYE MOLECULES

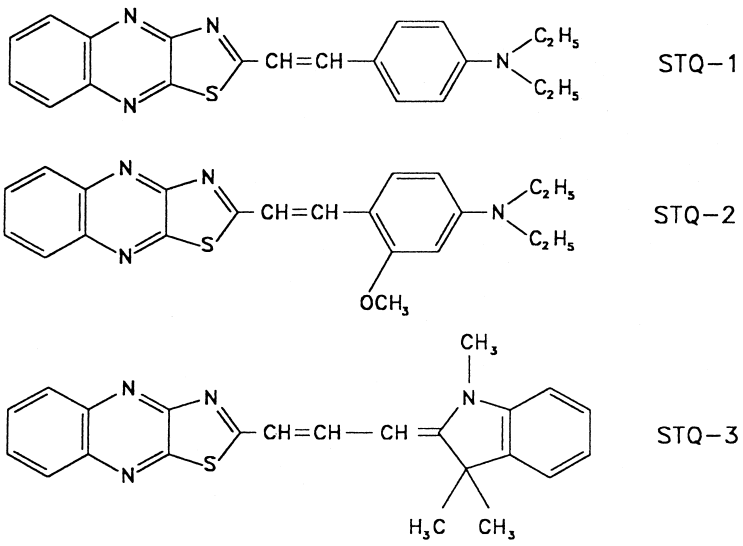

Fig. 1. Molecular structures of STQ-1, STQ-2 and STQ-3 dyes.

(pH 7.4). Aliquots of the dye solution in ethanol (1 mM) were added to the protein/micelle/membrane solution and stirred for 15 min to give a final concentration of the dye of ~10 μM in the sample.

The absorption and steady-state fluorescence experiments were done using Shimadzu UV2100, Spex Fluorolog 1681 and Shimadzu RF540 spectrometers, respectively. The time-resolved fluorescence decay measurements were made using a high repetition rate picosecond laser coupled to a time-correlated single photon counting spectrometer described elsewhere [14], currently using a microchannel plate photomultiplier (Hamamatsu 2809) and a personal computer for data acquisition and analysis. The sample was excited in the blue absorption band of the dye (380–400 nm region) by vertically polarized picosecond laser pulses (frequency doubled Ti-sapphire laser) and the emission was collected (at the peak in 580–630 nm region) through an emission polarizer oriented at the magic angle of 54.7° with respect to the excitation polarization. The full width at half maximum of the instrument response function was approximately 200 ps. Typical photon count rate for fluorescence decay measurements was 4000–5000 s^{-1} (~0.5% of the excitation rate) and the typical peak count was 10 000. The fluorescence decays were fitted to single or multiexponential functions by a standard procedure [14].

The fluorescence quantum yields for the dyes in ethanol were determined as follows. The fluorescence spectrum of a dilute (<25 μM) dye solution was recorded by excitation at the absorption peak. The fluorescence spectrum was corrected for the variation of the quantum efficiency of the photomultiplier (Hamamatsu R928). Similarly, a corrected fluorescence spectrum was obtained for a dilute rhodamine 101 in ethanol by excitation at its absorption peak of 420 nm. The quantum yield of the dye (ϕ_{dye}) was calculated using the equation

$$\phi_{dye} = \phi_{ref} \frac{I_{dye} A_{ref}}{I_{ref} A_{dye}}, \quad (1)$$

ϕ_{ref} is the fluorescence quantum yield of reference (rhodamine 101) sample in ethanol which is 1.0 [15], A_{dye} and A_{ref} are the absorbances of the dye and reference samples at their excitation wavelengths, I_{dye} and I_{ref} are the areas of the corrected fluorescence spectra (plotted in frequency scale) for the dyes and reference samples.

The electrochemical measurements were carried out using a potentiostat/galvanostat (EG and G PAR, Model 273A). A glassy carbon microelectrode (area: 0.06 cm^2) was used as the working electrode. A silver wire and Pt gauze were used as the quasi-reference and the counter electrode, respectively. Cyclic voltamograms of the STQ dyes were recorded in dichloromethane containing 0.1 M tetrabutyl ammonium perchlorate (TBAP). The solution was degassed by bubbling argon gas (99.992% purity, IOLAR grade from Indian Oxygen) through the solution. The potential was swept from 0 to −1.5 to + 1.5 V and back to 0 V with the sweep rate of 100 mV/s to record the current–voltage curve. After each experiment, the glassy carbon electrode was first washed with water, then cleaned by polishing it using 0.05 μm alumina powder. It was sonicated for about 5 min and then used for further experiments. Ferrocene $E^0(Ox) = 0.71 \pm 0.03$ V vs. NHE [16]) was used as the standard to determine the reference potential of Ag wire vs. NHE.

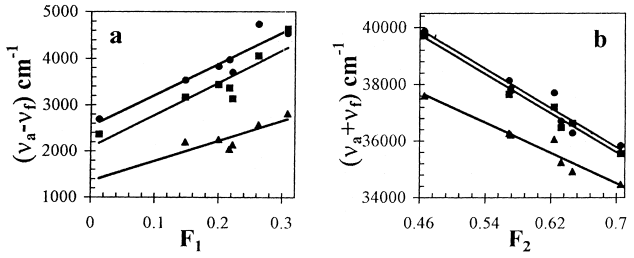

Fig. 2. (a) Plot of $(\nu_a - \nu_f)$ against the polarity parameter $F_1 \equiv \{(\varepsilon-1)/(2\varepsilon+1)-(n^2-1)/(2n^2+1)\}$ (see Eq. (2)) for (●) STQ-1, (■) STQ-2 and (▲) STQ-3. (b) Plot of $(\nu_a + \nu_f)$ against the polarity parameter $F_2\{\equiv (\varepsilon-1)/(2\varepsilon+1)+(n^2-1)/(2n^2+1)\}$ (see Eq. (3)) for (●) STQ-1, (■) STQ-2 and (▲) STQ-3.

Semiempirical quantum chemical calculations were performed using MOPAC software version 6.0 on a Pentium PC. The results of heat of formation for the hydrogen bonding/van der Waals complexes of NH_3/H_2O, H_2O/CH_3OH and $HCOOH/NH_3$ reported in literature [17] were reproduced using AM1 Hamiltonian for geometry optimization.

3. Results

The absorption and fluorescence emission spectra of STQ-1, STQ-2, and STQ-3 were measured in several organic solvents (methanol, dichloromethane (DCM), chloroform, dimethylsulphoxide (DMSO), ethylacetate, toluene, and 2-octanol). The spectra showed considerable spectral shifts in these organic solvents. The spectral shift is correlated with the polarity parameters (dielectric constant and refractive index) of the solvent. Fig. 2a shows the plots of $(\nu_a - \nu_f)$ versus the solvent polarity parameter [18] for the three dyes in seven solvents. The plots showed linear correlation that is in good agreement with the Lippert–Mataga equation [18]:

$$(\nu_a - \nu_f) = \frac{2(\mu_e - \mu_g)^2}{hca^3}\left(\frac{\varepsilon-1}{2\varepsilon+1} - \frac{n^2-1}{2n^2+1}\right) + K, \quad (2)$$

ν_a and ν_f are the peak absorption and emission (steady-state fluorescence) frequencies per centimetre, μ_e and μ_g the dipole moment of the dye in excited and ground state, ϵ and n the dielectric constant and refractive index of the solvent, respectively, h the Planck's constant, c the speed of light and a the Onsager cavity radius for the dye molecule. K is a constant. The model of dipole in a dielectric medium [18] that is used to derive Eq. (2) also gives Eq. (3) for the sum of ν_a and ν_f:

$$(\nu_a + \nu_f) = -\frac{2(\mu_e^2 - \mu_g^2)}{hca^3}\left(\frac{\varepsilon-1}{2\varepsilon+1} + \frac{n^2-1}{2n^2+1}\right) + K', \quad (3)$$

where K' is a constant. The positive sign in the term for the solvent polarity parameter in Eq. (3) may be noted. $(\nu_a - \nu_f)$ and $(\nu_a + \nu_f)$ were plotted against the respective solvent polarity parameter $F_1 = \{(\varepsilon-1)/(2\varepsilon+1)-(n^2-1)/(2n^2+1)\}$ of Eq. (2) and $F_2 = \{(\varepsilon-1)/(2\varepsilon+1)+(n^2-1)/(2n^2+1)\}$ of Eq. (3) in Fig. 2a and b for all three dyes, respectively. The plots showed satisfactory linear correlation as predicted by the above equations. The slopes of the two plots were used to calculate the ratio of the dipole moments (μ_e/μ_g).

The ground state dipole moments of the dye molecules STQ-1, STQ-2 and STQ-3 were calculated using quantum chemical calculations using the molecular orbital package MOPAC (version 6). The calculations were done for at least 10–20 randomly chosen initial geometry of the standard molecular structure and the values for the low-energy stable structure were taken. The dipole moments of the excited state were calculated for STQ-1, STQ-2 and STQ-3 using calculated value of μ_g and the value of (μ_e/μ_g). It may be noted that no assumption was made on the cavity radius a to obtain the ground and excited state dipole moments. The values of (μ_e/μ_g), μ_g and μ_e are given in Table 1 together with other molecular properties.

The electrochemical reduction and oxidation potentials for the dyes were determined by cyclic voltammetry using glassy carbon electrode in dichloromethane. The one electron oxidation of STQ-1, STQ-2 and STQ-3 occurs in the range of 0.93–1.00 V vs. NHE. The one electron reduction of STQ-1, STQ-2 and STQ-3 occurs in the range of −0.90 to −1.03 V vs. NHE. The electrochemical oxidation and reduction peaks were quasi-reversible indicating that the oxidized and reduced dye molecules are kinetically unstable.

The fluorescence decays of all the dyes were measured in several organic solvents. The fluorescence decay of STQ-1, STQ-2 or STQ-3 is one exponential in several solvents and the fluorescence lifetimes are given in Table 2. The fluorescence decays of STQ-1, STQ-2 and STQ-3 in 2-octanol and organized molecular assemblies were either two or three

Table 1
Molecular and photophysical properties of STQ dyes

Dye	Molecular weight	Melting Point°C	log (ϵ) (M^{-1} cm^{-1})[a]	λ_{abs} (nm)[b]	λ_{em} (nm)[b]	Quantum yield[c]	μ_e/μ_g	μ_g (Debye)	μ_e (Debye)	E^0 (Ox) (V)[d]	E^0 (Red) (V)[d]
STQ-1	360.4	230	4.94	490	630	0.36	2.26	3.28	7.43	0.998	−0.907
STQ-2	390.5	156	4.80	485	625	0.32	2.23	4.51	10.51	0.993	−0.927
STQ-3	384.5	205	4.87	530	623	0.75	1.96	2.67	5.22	0.933	−1.027

[a] Solvent: chloroform.
[b] Solvent: methanol.
[c] Solvent: ethanol.
[d] V vs. NHE solvent: dichloromethane; glassy carbon electrode.

Table 2
Fluorescence lifetime(s) and amplitude(s) of STQ dyes in organic media[a]

Solvent/medium	STQ-1 (ns)	STQ-2 (ns)	STQ-3 (ns)
Methanol	0.05	0.04	0.18
Chloroform	1.31	0.97	1.08
DCM	1.62	1.29	0.99
DMSO	0.42	0.41	1.04
Toluene	0.27	0.27	0.11
Ethyl acetate	1.36	0.96	0.92
2-Octanol	0.41 (0.62)	0.41 (0.55)	0.51 (0.61)
	1.94 (0.38)	1.67 (0.45)	1.88 (0.39)
SDS micelle	0.32 (0.98)	0.18 (0.74)	0.62 (0.93)
	0.65 (0.02)	0.50 (0.26)	1.62 (0.07)
Lysozyme	0.85 (0.85)	1.01 (0.76)	1.14 (0.64)
	2.69 (0.15)	3.05 (0.24)	2.81 (0.36)
EggPC	0.35 (0.22)		
	0.85 (0.46)		
	1.62 (0.32)		

[a] Excitation at 380–400 nm. Emission measured at the peak of the emission spectrum in the range 580–630 nm. Reduced chi-square values for all decays is in the range $0.9 < \chi^2 < 1.1$.

exponentials and the lifetimes and amplitudes are also given in Table 2. The amplitudes of the lifetimes were wavelength dependent in 2-octanol, SDS micelle and in eggPC membrane but wavelength independent in protein (lysozyme). The results of a detailed analysis of the multiexponential decays are described subsequently.

The temperature dependence of the single exponential fluorescence decay of STQ-1 was examined in DCM and DMSO. The fluorescence decays in DMSO and DCM at 5, 15, 25, 35 and 45°C are shown in Figs. 3 and 4, respectively. The decays were fitted well to the single exponential

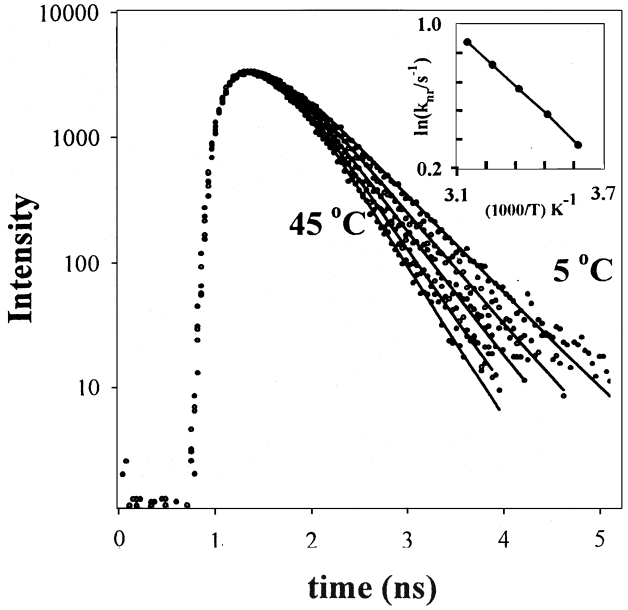

Fig. 3. Temperature dependence of the fluorescence decay of STQ-1 in DMSO, at 5, 15, 25, 35 and 45°C. Solid line through the decay is the fit for one exponential decay function. Inset in the figure shows the plot of $\ln(k_{nr}/s^{-1})$ vs. $1000/T$ (K^{-1}) (see text).

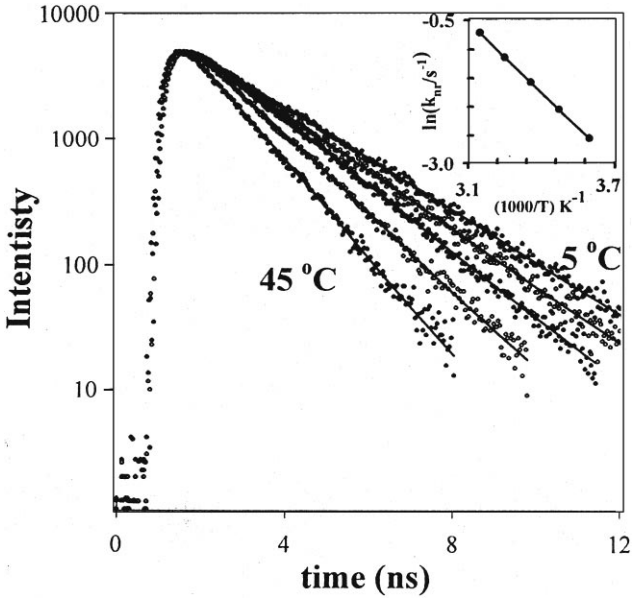

Fig. 4. Temperature dependence of the fluorescence decay of STQ-1 in dichloromethane at 5, 15, 25, 35 and 45°C. Solid line through the decay is the fit for one exponential decay function. Inset in the figure shows the plot of $\ln(k_{nr}/s^{-1})$ vs. $1000/T$ (K^{-1}) (see text).

decay equation (solid lines in the figures). The fluorescence lifetime decreased from 2.10 ns (5°C) to 1.124 ns (45°C) in DCM and in DMSO the decrease was from 0.562 ns (5°C) to 0.35 ns (45°C). The percentage decrease in steady-state fluorescence intensity with temperature in this range was approximately the same as the percentage decrease in lifetime. The change in the refractive index in this temperature range is too small to significantly reduce the radiative rate [19]. The temperature dependence of lifetime is therefore attributed to the temperature dependence of the nonradiative rate (k_{nr}) for the dye in the excited state. The activation energy (ΔE) for the nonradiative process was obtained based on the equation, $k_{nr} = k_{nr}{}^0 \exp(-\Delta E/RT)$, from the best linear fit of $\ln(k_{nr})$ vs. $1/T$ (°K), where $k_{nr} = \tau_f{}^{-1} - k_r$. The insets in Figs. 3 and 4 show the best linear fits for the data in DCM and DMSO for the values of $k_r = 0.39\,ns^{-1}$ (DCM) and $k_r = 0.40\,ns^{-1}$ (DMSO).

3.1. Multiexponential fluorescence in octanol and complex media

The STQ dyes readily bind to the protein (lysozyme) and the organized molecular assembly of micelle (SDS) or bilayer membrane (eggPC). The absorption and fluorescence spectra of the dyes in these organic media are qualitatively similar to those observed in the polar solvent methanol. The results of detailed analysis of double exponential fluorescence decays in 2-octanol and organized molecular assemblies are described below.

The fluorescence decay of STQ-1 in 2-octanol at different wavelengths in the emission spectrum was double exponen-

tial and the lifetimes were reasonably constant in the entire spectrum: $\tau_{Short} = 0.40 \pm 0.15$ and $\tau_{Long} = 1.94 \pm 0.08$ ns. The variation of the amplitudes (α_S and α_L) of the short and long lifetimes with the wavelength for the two lifetimes are shown in Fig. 5b. The amplitude for the short lifetime, α_S was positive for $\lambda < 630$ nm and was negative for $\lambda > 630$ nm. The wavelength dependent amplitudes and steady-state emission spectrum were used to construct the spectra of the two species (see Section 4 for equations) associated with the short and long lifetimes. The spectra are shown in Fig. 5a.

The fluorescence decays of STQ-1 in protein and micelle were also double exponential at different wavelengths in the emission spectrum. The fluorescence lifetimes were reasonably constant in the entire spectrum: $\tau_{Short} = 0.85 \pm 0.15$ and $\tau_{Long} = 2.69 \pm 0.05$ ns (protein), $\tau_{Short} = 0.32 \pm 0.1$ and $\tau_{Long} = 1.65 \pm 0.15$ ns (micelle). In the case of lipid membrane, two exponentials were not adequate and it was necessary to consider three exponential functions which gave lifetimes that were constant at all emission wavelengths: $\tau_{Short} = 0.35 \pm 0.12$, $\tau_{Middle} = 0.85 \pm 0.15$ and $\tau_{Long} = 1.62 \pm 0.12$ ns. The variations of the amplitudes for the two (protein and micelle) and three (membrane) lifetimes with the wavelength are shown in Fig. 5d, f and h. The wavelength dependent amplitudes and steady-state emission spectrum are used to construct the spectra of the two or three species (see Section 4 and Appendix A) associated with the lifetimes that are also shown in Fig. 5c, e and g.

4. Discussions

Thiazolo quinoxaline based styryl dyes studied here have several characteristics that are similar to other styryl dyes reported in literature [4–10]. (Some styryl dyes are also called hemicyanine and amino styryl pyridinium dyes.) Most of the styryl dyes are charged molecules but the STQ dyes used in this study are neutral molecules. These styryl dyes have a common structural feature, namely an electron donor and electron acceptor moiety on either side of a styryl double bond. The trans isomer of the styryl dye is the stable one in the ground state. The intramolecular electron donor–acceptor moieties in the styryl dye make it more sensitive to solvent and host environment. The structures of the three styryl thiazolo quinoxaline (STQ) dyes (Fig. 1) have a common electron acceptor group (thiazolo quinoxaline) but differ in the aromatic amine moiety. The STQ dyes are strongly coloured and highly fluorescent molecules. The fluorescence quantum yield of STQ-3 was the highest among the three dyes (Table 1). The solubility in organic solvents and a high binding affinity to membranes and proteins are useful properties of the dyes for biological applications and electronic/photonic molecular thin film devices. The relatively low redox potentials (±1 V vs. NHE) is favourable for electron and hole transfer from electrode to the film.

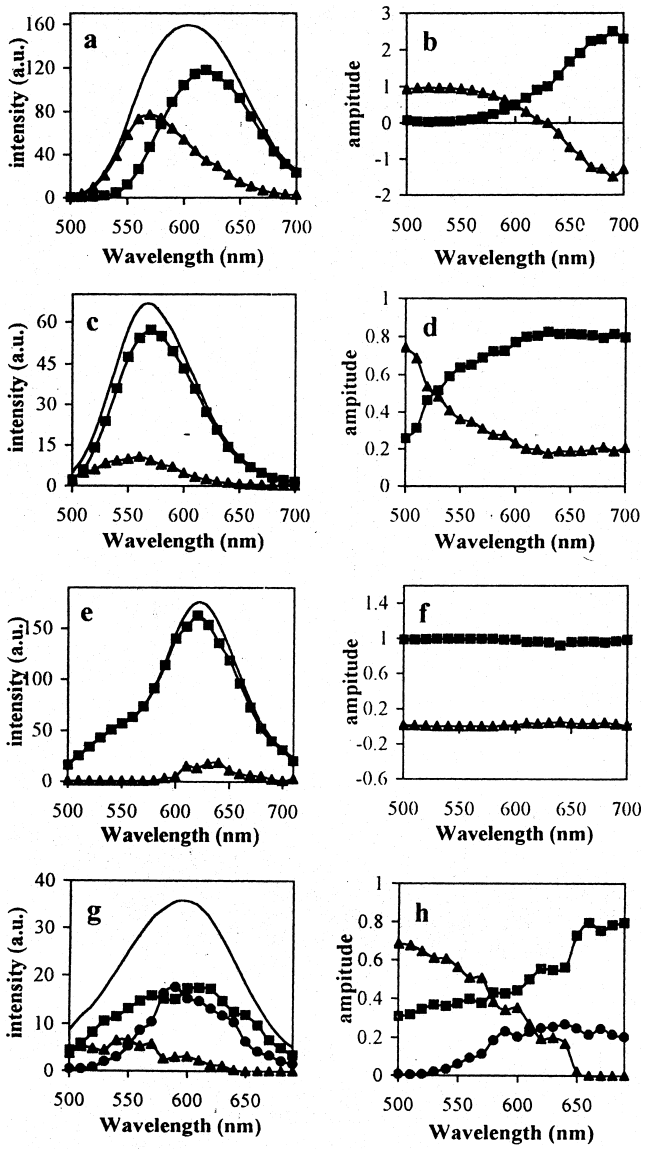

Fig. 5. Spectra of the multiple species in the emission spectrum of STQ-1 in organized molecular assemblies and wavelength dependence of the amplitudes of the two or three lifetimes; (a, b) 2-octanol: steady-state spectrum (solid line) and the spectra of the (▲) unrelaxed and (■) relaxed species of STQ-1, and variation of the amplitudes of the (▲) short ($\tau_S = 0.41 \pm 0.15$ ns) and (■) long ($\tau_L = 1.94 \pm 0.08$ ns) lifetimes with wavelength; (c, d) SDS micelle: steady-state spectrum (solid line) and the spectra of the two species associated with of the (▲) short ($\tau_S = 0.32 \pm 0.1$ ns) and (■) long ($\tau_L = 0.65 \pm 0.15$ ns) lifetimes in micelle of STQ-1 and variation of the corresponding amplitudes with wavelength; (e, f) lysozyme: steady-state spectrum (solid line) and the spectra of the two species in different sites with (▲) short ($\tau_S = 0.85 \pm 0.15$ ns) and (■) long ($\tau_L = 2.69 \pm 0.05$ ns) lifetimes in the protein of STQ-1, and variation of the corresponding amplitudes with wavelength; (g, h) eggPC bilayer membrane: steady-state spectrum (solid line) and the spectra of the three species in different sites in the membrane with (▲) short ($\tau_S = 0.35 \pm 0.12$ ns), (●) middle ($\tau_M = 0.85 \pm 0.15$ ns) and (■) long ($\tau_L = 1.62 \pm 0.12$ ns) of STQ-1, and variation of the corresponding amplitudes with wavelength.

The STQ dyes absorb strongly in the visible region with a molar extinction coefficient greater than $6 \times 10^4\,M^{-1}\,cm^{-1}$. The absorption and emission spectra of the STQ dyes are sensitive to the solvent or host environment which is attributable to the difference in the dipole moment in the ground and excited state (Table 1). As described in Section 3, the values of μ_e and μ_g were determined using spectral shift and the theoretical value for μ_g. The difference in the dipole moment $\Delta\mu$ is 2.5–6 Debye for the different STQ dyes. A value for cavity radius a in Eq. (2) is sometimes assumed for calculating $\Delta\mu$ for other styryl dyes [8]. On the other hand, it is possible to calculate the cavity radius using μ_e, μ_g and the slopes of the plot in Fig. 2a or b. The calculated values of cavity radius for STQ-1, STQ-2 and STQ-3 are in the range of 2–3 Å and thus the cavity diameter is in the range of 4–6 Å. This value is rather small compared to the molecular length of the STQ dyes which is about 15–17 Å, and comparable to the length of the short axis. It is interesting to comment on the significance, if any, of the cavity diameter obtained as above using experimental results and Eqs. (2) and (3).

The model used to derive Eqs. (2) and (3) is based on a point dipole in a spherical cavity. Most organic fluorescent molecules for which these equations are applied are neither point dipoles nor spherical in shape. On the other hand, non-uniform distribution of charge in the ground and excited state gives rise to dipole and higher order moments and energy minimization occurs in the electrostatic force field of dipolar solvent molecules. A realistic model of the solvent structure around the molecular dipole is very complex and the simple model such as that used to obtain Eqs. (2) and (3) are only approximations. Alternative realistic models are necessary.

We have examined the possible meaning for the small cavity radius for STQ dyes by correlating with the charge/electron density distribution in the ground and excited state of STQ-1 dye. It was observed from theoretical calculations that major changes in net atomic charges occur only in a few atoms of the dye in the vicinity of the styryl bond. Fig. 6 shows the charge distribution in the atoms for ground and excited state (in braces). Large changes (>0.12) in the absolute value of net charge were observed for the atoms that are shown in bold in Fig. 6. It is reasonable therefore to expect that this part of the molecule plays a dominant role in the solvation dynamics because of the large changes in atomic charges. Interestingly, the length of this part of the molecule (Fig. 6) is found to be 4.3 Å, which is close to the calculated value of 'cavity' diameter. It is worth investigating if such a correlation exists for other styryl dye molecules.

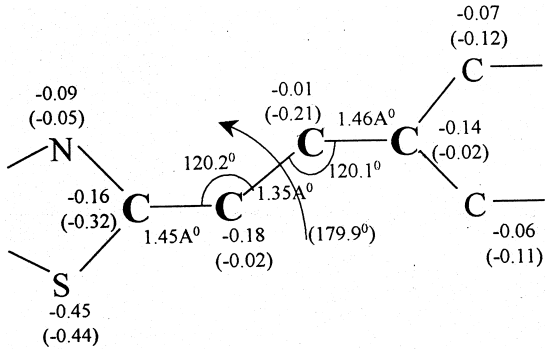

Fig. 6. Net charges on the atoms near the styryl group of STQ-1, bond distances and angles in the ground state. The values of net charge on the atoms in the excited state are given in brackets.

4.1. Dye–solvent complex in DCM

In solvents of low viscosity the fluorescence decay of STQ dyes is single exponential (Table 2). The temperature dependence of the lifetime in DCM and DMSO was ascribed to the temperature dependence of the nonradiative rate. The activation energies in DCM and DMSO were determined to be 34.0 and 10.7 kJ/mol, respectively. The activation energy for the nonradiative process of styryl dyes, including stilbenes, in viscous solvents is understood in terms of intramolecular dynamics (e.g., rotation about a bond). According to Kramer's theory [20], in the limit of viscosity-controlled Smoluchowski limit

$$k_{nr} \propto \left(\frac{1}{\eta^{\alpha}}\right) \exp\left(\frac{-E^0}{RT}\right), \tag{4}$$

where E^0 is the activation barrier for the intramolecular dynamics and $\alpha < 1$. The temperature dependence of viscosity itself is given by the equation [21]

$$\eta = \eta_0 \exp\left(\frac{E_a}{RT}\right), \tag{5}$$

where η_0 is a constant and E_a the activation energy for the mobility of a solvent molecule in the solvent. Combining Eqs. (4) and (5), we get

$$k_{nr} \propto (\eta_0)^{-\alpha} \exp\left(-\frac{\alpha E_a + E^0}{RT}\right). \tag{6}$$

As described in Section 3, $\Delta E = (\alpha E_a + E^0)$ was determined from the experimental data of temperature dependence of fluorescence lifetime of STQ-1 in DCM (ΔE = 34.0 kJ/mol) and DMSO (ΔE = 10.7 kJ/mol). Using the viscosity data [22] in the temperature range 5–50°C for DCM and DMSO one obtains E_a = 6.6 kJ/mol for DCM and E_a = 13.7 kJ/mol for DMSO. Comparison of the values of ΔE and E_a in DMSO indicates that E^0 becomes negligible for $\alpha \sim 0.8$ which implies that the nonradiative process in DMSO is a barrierless one and the rate is determined by viscosity alone. On the other hand, a comparison of the values of ΔE and E_a in DCM suggests that E^0 is in the range 27.4–16.6 kJ/mol for $1 > \alpha > 0$. The significantly higher value for E^0 in DCM may be interpreted to suggest that a barrier exists for the intramolecular dynamics of the dye. A barrier could presumably arise due to complex formation

involving the dye and the solvent. The possibility of such a dye–solvent complex and its geometry were investigated by theoretical calculations that are described below.

The theoretical calculations of energy minimization and geometry optimization of the dye STQ-1, solvent DCM and dye–solvent complexes of different geometries were carried out using MOPAC. The calculations showed that the charge of the H-atom in DCM is positive (+0.129) and that of the Cl-atom is negative (−0.077). The calculations for STQ-1 showed that the net atomic charges were significantly different in ground and excited atoms for a few atoms near the styryl bond. Maximum negative charge (−0.31 in the ground state and −0.27 in the excited state) was observed at the N-atom of the *N*,*N*-diethyl amino group. Complex formation between the dye and DCM is therefore likely by H-bonding interaction between DCM and the dye. Geometry optimization and energy calculations showed a stable complex formation (heat of formation is −0.71 kJ/mol) involving H-bonding with N-atom of the *N*,*N*-diethyl amino group of the STQ-1 dye. Interestingly, the heat of formation for a complex formed between Cl-atom of DCM and H-atom of ethyl group was much higher at −2.05 kJ/mol. It is possible therefore that more than one solvent molecule is involved in the dye–solvent complex. A similar calculation for the interaction between CCl_4 and the STQ-1 dye gave a heat of formation of only −0.11 kJ/mol. Thus, the theoretical calculations are in favour of a dye–DCM complex involving the H and Cl atoms of the DCM. The large activation energy observed in this solvent ban be rationalized by the formation such dye–solvent complexes.

4.2. Multiexponential decay in complex organic media

The dipole moments of the STQ dyes in the excited state were calculated to be 5.2–10.5 Debye which is larger than that in the ground state (Table 1). The fluorescence spectrum of the dye in a polar solvent undergoes a red shift because of the dipolar interaction of the excited state with the solvent, which is generally termed as solvation dynamics. The interaction involves reorientation of the solvent molecules around the dye and the relaxation time depends upon the viscosity of the solvent. The excitation, relaxation of the excited state by solvent interaction and emission from unrelaxed and relaxed states are described by a well-known model of excited state solvation dynamics [18] which is shown in Fig. 7. In Fig. 7, $M_s{}^*$ is the initial excited state of the dye where the solvent molecules are in the same orientational distribution as in the ground state and $M_{s'}{}^*$ is the relaxed state where the orientational distribution of solvent molecules is different. k is the rate of solvent relaxation which is viscosity dependent. In solvents of low viscosity the relaxation rate k is very fast and the fluorescence emission is observed only from the relaxed state. The fluorescence decay in a low viscosity, polar solvent is therefore single exponential. In polar solvents of high viscosity the relaxation rate k is slow and emissions from both $M_s{}^*$ and $M_{s'}{}^*$ are observed. In

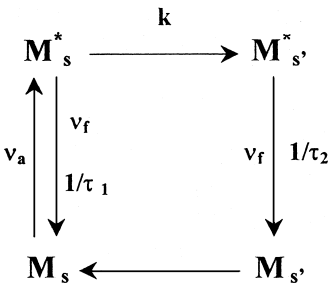

Fig. 7. Solvent relaxation model. M_s, $M_{s'}$ $M_s{}^*$ and $M_{s'}{}^*$ are the solvated dye molecule in the ground state (relaxed), ground state (unrelaxed), excited state (unrelaxed) and excited state (relaxed), respectively. ν_a and ν_f are the absorption and emission frequencies. $1/\tau_1$ is the sum of radiative and nonradiative rates of $M_s{}^*$, $1/\tau_2$ is the sum of radiative and nonradiative rates of $M_{s'}{}^*$ and k is the rate constant of solvent relaxation.

such a case, the fluorescence decay is double exponential with the lifetime of $(\tau_1{}^{-1} + k)^{-1}$ (due to $M_s{}^*$) and τ_2 (due to $M_{s'}{}^*$). Further, the solvent relaxation model implies that the emission spectrum of $M_{s'}{}^*$ is red shifted with respect to $M_s{}^*$ and hence the amplitudes of the two lifetimes vary with emission wavelength. A negative amplitude for the lifetime associated with $M_s{}^*$ at longer emission wavelengths is a confirmatory evidence for the solvent relaxation model.

Double exponential fluorescence decays were observed for STQ dyes in 2-octanol and in organized molecular assemblies of micelle and protein (Table 2). The results of a detailed analysis of the fluorescence decays of STQ-1 in these organic media at different emission wavelengths are shown in Fig. 5a–h. Examination of the wavelength dependence of amplitudes in Fig. 5b, d, f and h suggests that the trend in octanol (negative amplitudes at long emission wavelengths) is different from other media. In the case of octanol, the amplitudes for the short lifetime decreased with the emission wavelength and became negative at extreme red end of the emission spectrum. This trend is in complete agreement with the solvent relaxation model for the excited state of the dye described above. The spectra of the two species $M_s{}^*$ and $M_{s'}{}^*$ can be calculated for this model of excited state kinetics using steady-state emission spectrum (see Appendix A; Eqs. (A.6) and (A.7)). The computed spectra associated with the two species, $M_s{}^*$ and $M_{s'}{}^*$ are shown in Fig. 5a. The spectrum of the relaxed species $M_{s'}{}^*$ is red shifted.

In the organized molecular assembly of micelle the double exponential decay parameters were different from those observed in 2-octanol. The fluorescence lifetimes were unchanged but the amplitudes varied with emission wavelength as shown in Fig. 5d. The lifetimes of both the species (0.32 and 0.60 ns) are substantially less in SDS micelle compared to protein or membrane. There was no negative amplitude at any wavelength and hence the two species are not kinetically coupled in the fluorescence time scale. Two different sites of solubilization for the dye in the micelle are therefore indicated. The emission spectra for the two species are calculated using Eqs. (A.12) and (A.13) (Appendix A).

The spectrum of the long lifetime component is red shifted (Fig. 5c).

The fluorescence decay analysis of STQ-1 bound to the protein gave similar results as in SDS micelle but differed quantitatively. The lifetimes were larger (0.85 and 2.69 ns) and the amplitudes of the two lifetimes were unchanged with the emission wavelength (Fig. 5f). Absence of negative amplitude at any wavelength indicated that the two species are not kinetically coupled in the fluorescence time scale. The ratio of the two amplitudes at different emission wavelengths varied little suggesting that the spectra of the two species are similar (Fig. 5f). The results indicate two different sites of solubilization with identical environment for the dye in the protein and the dye is probably quenched in one site.

The fluorescence decay of STQ-1 in lipid membrane at all emission wavelengths was best fitted to three exponential functions: $\tau_{\text{Short}} = 0.35 \pm 0.12$ $\tau_{\text{Middle}} = 0.85 \pm 0.15$ and $\tau_{\text{Long}} = 1.62 \pm 0.12$ ns. The amplitudes of the three lifetimes varied as shown in Fig. 5h. The amplitude of the 0.35 ns component decreased with increasing wavelength. The amplitude of 0.85 and 1.62 ns components increased steadily with wavelength (Fig. 5h). There was no negative amplitude at long wavelengths for the short component. The results are consistent with a model involving three solubilization sites for the dye molecule, which are not kinetically coupled. The spectra for the three species are different (Fig. 5g).

The results and discussion of fluorescence spectra and fluorescence decay of STQ dyes in different organic media indicates that the photophysics of the dye is sensitive to the host environment. Organized molecular assemblies provide multiple environments for the dye and thus the fluorescence is more complex than in homogeneous organic media.

5. Conclusions

The photophysics of a new class of styryl dyes has been studied in organic media. The ground and excited state dipole moments have been determined. The dye forms a dye–solvent complex in dichloromethane. The multiexponential fluorescence decay of the dye in octanol is due to solvation dynamics in excited state. However, the multiexponential decay in organized molecular assemblies (micelle, membrane and protein) is attributed to multiple solubilization sites for the dye.

Appendix A

A.1. Solvent relaxation model

A two-state solvent relaxation model as shown in Fig. 7 predicts that the fluorescence decay at any emission wavelength is proportional to the sum of the population decays of $M_s{}^*$ and $M_{s'}{}^*$.

$$I_\lambda(t) = a_\lambda [M_s{}^*]_t + b_\lambda [M_{s'}{}^*]_t, \tag{A.1}$$

where a_λ and b_λ are the intensity contributions of the two species at λ, and

$$[M_s{}^*]_t = C_0 \exp\left\{-t\left(k + \frac{1}{\tau_1}\right)\right\}, \tag{A.2}$$

$$[M_{s'}{}^*]_t = C_0 \left[\frac{k}{k + 1/\tau_1 - 1/\tau_2}\right] \times \left[\exp\left(\frac{-t}{\tau_2}\right) - \exp\left\{-t\left(k + \frac{1}{\tau_1}\right)\right\}\right]. \tag{A.3}$$

C_0 is the concentration of $M_s{}^*$ at $t = 0$. Replacing $(k + 1/\tau_1) = 1/\tau_{S\,(\text{short})}$ and $\tau_2 = \tau_{L\,(\text{long})}$, one gets

$$I_\lambda(t) = x_\lambda \exp\left(\frac{-t}{\tau_S}\right) + y_\lambda \left[\exp\left(\frac{-t}{\tau_1}\right) - \exp\left(\frac{-t}{\tau_L}\right)\right], \tag{A.4}$$

or

$$I_\lambda(t) = \alpha_\lambda \exp\left(\frac{-t}{\tau_S}\right) + \beta_\lambda \exp\left(\frac{-t}{\tau_L}\right), \tag{A.5}$$

where $x_\lambda = \alpha_\lambda + \beta_\lambda$, and $y_\lambda = \beta_\lambda$. It is recognized that α_λ can be negative at long emission wavelengths when $y_\lambda > x_\lambda$. According to Eq. (A.4), the contribution to the steady-state intensity (I^{ss}) at λ will be in the ratio of $x_\lambda \tau_S : y_\lambda(\tau_L - \tau_S)$ for the two species $M_s{}^*$ (associated with τ_S) and $M_{s'}{}^*$ (associated with τ_L), respectively. The individual spectrum of the two species $M_s{}^*$ and $M_{s'}{}^*$ are computed using Eqs. (A.6) and (A.7).

$$I_{M_s{}^*} = I_\lambda^{ss} \frac{x_\lambda \tau_S}{x_\lambda \tau_S + y_\lambda(\tau_L - \tau_S)}. \tag{A.6}$$

$$I_{M_{s'}{}^*} = I_\lambda^{ss} \frac{y_\lambda(\tau_L - \tau_S)}{x_\lambda \tau_S + y_\lambda(\tau_L - \tau_S)}. \tag{A.7}$$

A.2. Multiple site model

The model of two (or more) solubilization sites for the dye in the organized molecular assembly predicts that the fluorescence decay at any emission wavelength is proportional to the sum of the population decays of $M_1{}^*$ and $M_2{}^*$,

$$I_\lambda(t) = a_\lambda [M_1{}^*]_t + b_\lambda [M_2{}^*]_t, \tag{A.8}$$

where a_λ and b_λ are the intensity contributions of the two species at λ, and

$$[M_1{}^*]_t = C_1 \exp\left(\frac{-t}{\tau_1}\right), \tag{A.9}$$

$$[M_2{}^*]_t = C_2 \exp\left(\frac{-t}{\tau_2}\right). \tag{A.10}$$

C_1 is the concentration of $M_1{}^*$ and C_2 the concentration of $M_2{}^*$ at $t = 0$,

$$I_\lambda(t) = \alpha_\lambda \exp\left(\frac{-t}{\tau_1}\right) + \beta_\lambda \exp\left(\frac{-t}{\tau_2}\right). \quad \text{(A.11)}$$

It is recognized that α_λ and β_λ are positive at all emission wavelengths. According to Eq. (A.11), the contribution to the steady-state intensity (I^{ss}) at λ will be in the ratio of $\alpha_\lambda\tau_1$:$\beta_\lambda\tau_2$ for the two species $M_1{}^*$ and $M_2{}^*$, respectively. The individual spectrum of the two species $M_1{}^*$ and $M_2{}^*$ are computed using Eqs. (A.12) and (A.13):

$$I_{M_1{}^*} = I_\lambda^{ss}\frac{\alpha_\lambda\tau_1}{\alpha_\lambda\tau_1 + \beta_\lambda\tau_2}, \quad \text{(A.12)}$$

$$I_{M_2{}^*} = I_\lambda^{ss}\frac{\beta_\lambda\tau_2}{\alpha_\lambda\tau_1 + \beta_\lambda\tau_2}. \quad \text{(A.13)}$$

References

[1] A.P. Alivastos, P.F. Barbara, A.W. Castleman, J. Chang, D.A. Dixon, M.L. Klein, G.L. McLendon, J.S. Miller, M.A. Ratner, P.J. Rossky, S.I. Stupp, M.E. Thompson, Adv. Mater. 10 (1998) 1297.
[2] S. Miyata, H.S. Nalwa (Eds.), Organic Electroluminescent Materials and Devices, Gordon and Breach, Amsterdam, 1997.
[3] Special Issue on Organic Materials, Acc. Chem. Res. 32 (1999) 191.
[4] L.M. Loew, L.L. Simpson, Biophys. J. 34 (1981) 353.
[5] N. Ikeda, N. Mataga, U. Steiner, M.H. Abdel-Kader, Chem. Phys. Lett. 95 (1983) 66.
[6] H. Ephardt, P. Fromherz, J. Phys. Chem. 93 (1989) 7717.
[7] N.V. Visser, A. von Hoek, A.J.W.G. Visser, R.J. Clarke, J.F. Holzwarth, Chem. Phys. Lett. 231 (1994) 551.
[8] U. Narang, C.F. Zhao, J.D. Bhawalkar, F.V. Bright, P.N. Prasad, J. Phys. Chem. 100 (1996) 4521.
[9] B. Strehmel, H. Seifert, W. Rettig, J. Phys. Chem. 101 (1997) 2232.
[10] A. Mishra, R.K. Behera, B.K. Mishra, G.B. Behera, J. Photochem. Photobiol. A 116 (1998) 79.
[11] R.P. Haughland, Handbook of Fluorescent Probes and Research Chemicals, 6th Edition, Molecular Probes, PO Box 22010, Eugene, OR, USA (Chapter 14).
[12] D.W. Rangnekar, N.D. Sonawane, R.W. Sabnis, J. Heterocyclic Chem. 35 (1998) 1353–1356.
[13] M.M.G. Krishna, N. Periasamy, J. Fluoresc. 8 (1998) 81.
[14] N. Periasamy, S. Doraiswamy, G.B. Maiya, B. Venkataraman, J. Chem. Phys. 88 (1988) 1638.
[15] T. Karstens, K. Kobs, J. Phys. Chem. 84 (1980) 1871.
[16] W.C. Barrette, H.W. Johnson, D.T. Sawyer, Anal. Chem. 56 (1984) 1890.
[17] M.J.S. Dewar, E.G. Zoebisch, E.F. Healey, J.J.P. Stewart, J. Am. Chem. Soc. 107 (1985) 3902.
[18] J.R. Lakowicz, Principles of Fluorescence Spectroscopy, Plenum Press, New York, 1983, p. 190
[19] J.B. Birks, Photophysics of Aromatic Molecules, Academic Press, New York, 1970.
[20] G.R. Fleming, Chemical Applications of Ultrafast Spectroscopy, Oxford University Press, New York, 1986 (Chapter 6).
[21] P.W. Atkins, Physical Chemistry, 5th Edition, ELBS with Oxford University Press, Singapore, 1994, p. 833.
[22] Landoldt-Bornstein, Transport Phenomena I, Springer, Berlin, 1969, pp. 195, 245.